JOURNAL OF MATERIALS SCIENCE 33 (1998) 3121–3129

Functionally gradient superconducting foils by plasma spraying

J. H. CHEN*, M. F. BESSER, R. K. TRIVEDI, M. J. KRAMER, D. J. SORDELET
Ames laboratory USDOE, Iowa State University, Ames, IA 50011, USA
E-mail: zchen@gsut.edu.cn

Functionally gradient composite foils of Y–Ba–Cu–O and silver with a layer thickness of around 100 μm and certain flexibility, were produced by air plasma spraying. The superconducting phase is formed in sprayed composite foils only after annealing in flowing oxygen above 900 °C but can be improved by annealing first in argon at 850 °C prior to the oxygen annealing. The effect of argon pre-treatment was found to increase the grain size of $YBa_2Cu_3O_{7-\delta}$. The behaviour of the graded silver layer in improving the ductility and in the process of recovery of superconductivity of the sprayed coating was investigated.

1. Introduction

This study stemmed from two ideas: first to use the concept of functionally gradient (graded) material (FGM) [1] to manufacture flexible composite foils of $YBa_2Cu_3O_{7-\delta}$ (Y123) superconductor with uniform layers of a ductile metal (silver) to enhance the ductility of this brittle ceramic, and second to utilize some of the beneficial effects found in the Ag + Y123 composites [2–9].

Many researchers have shown the improvement in the superconducting transition temperature, T_c, in sprayed Y–Ba–Cu–O coatings after annealing them in flowing oxygen [10–15]. Neiser noted an improvement in T_c by argon pre-treatment [16]. However, there are still two problems to be solved: poor transport critical current, J_c, which is usually few hundreds of amperes per square centimetre or even lower in the presence of an applied magnetic field and persistent brittle behaviour. A partial melt/textured growth process has been used to raise J_c up to one order of magnitude higher than the original randomly orientated structure [17]. The other problem is the brittleness of the YBaCu–O coating which limits its use.

Silver was found to decrease cracking and increase the transport critical current in melt-processed Y123 [3,4]. Addition of silver significantly lowers the onset of melting in the $YBa_2Cu_3O_7$–$BaCuO_2$–CuO system [2].

In this work, an attempt was made to make plasma-sprayed Y123 coatings flexible by functionally graded silver layers. The behaviour of the silver layer in improving the ductility and in regaining the superconducting phase of sprayed coating has been discussed. In addition, the effect of argon pre-treatment on the superconductivity was investigated.

2. Experimental procedure

2.1. Materials

Feedstock for the plasma spraying was gas-atomized pure silver powder with particle size of +45 μm and an off-stoichiometric ceramic powder with cation ratios of Y : Ba : Cu 1 : 2 : 4.5 and particle size of −45 μm. Both powders were obtained from commercial sources, the silver from HJE Inc., and the Y123 ceramics powder from Metco (SC23) using a double HOSPING process. The mild steel plates without sandblasting were used as substrate, for easy detachment of sprayed coating, due to the large difference in thermal expansion coefficient between silver ($19 \times 10^{-6}\ K^{-1}$) and steel ($\sim 11 \times 10^{-6}\ K^{-1}$).

2.2. Plasma spraying

Functionally graded coatings of Y–Ba–Cu–O with silver were produced by spraying 20 μm thick layers of silver powder alternating with Y–Ba–Cu–O powder. This process sandwiched two layers of Y–Ba–Cu–O between three layers of silver for a total coating thickness of about 100 μm. The first layer of silver was sprayed on the cold mild steel substrate. For X-ray diffraction (XRD) analyses, coatings with two layers of silver powder sandwiched with two layers of Y–Ba–Cu–O powder were sprayed to leave the ceramic layer exposed to the X-rays.

The plasma spraying processes were carried out in an air atmosphere using a SG-100 gun made by Miller

*Senior visiting scientist of the International Institute of Theoretical and Applied Physics of Iowa State University working with Ames Laboratory of DOE. *Permanent address*: Gansu University of Technology, Lanzhou, Gansu 730050, People's Republic of China.

Thermal Inc. Two powder feeders were used to feed silver and Y–Ba–Cu–O powders individually (Fig. 1). The plasma spraying parameters and the arrangement of the sprayed layers are shown in Tables I and II, respectively. After spraying, coatings were detached from steel substrates using a razor blade and stored in a vacuum chamber.

2.3. Heat treatment of specimens

Three different procedures for heat-treating the deposited coating were used: (1) pre-treatment in argon, holding at 850 °C for 6 h in a pure argon atmosphere; (2) annealing in oxygen, holding at 920 °C for 24 h and then at 450 °C for 24 h in oxygen at a flow rate of $100\,cm^3\,min^{-1}$ through a silica tube of 60 mm diameter; (3) pre-treating in argon plus annealing in oxygen. The heating rate was $30\,°C\,min^{-1}$ and the cooling rate was $4\,°C\,min^{-1}$. Corresponding notations of the specimens are shown in Table III, including the as-sprayed specimens. All the specimens were kept in a vacuum chamber of 10^{-2} torr (1 torr = 133.322 Pa).

2.4. Measurements

The thicknesses of the sprayed foils detached from the substrates were measured first roughly using a micrometer and then more accurately from optical and scanning electron micrographs of cross-sections, using specimen S-3-3.

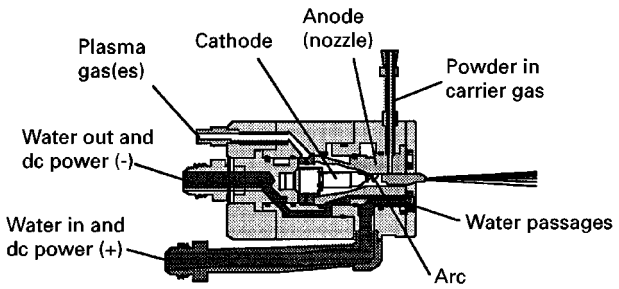

Figure 1 Schematic drawing of the plasma gun SG-100.

TABLE I Parameters of air plasma spraying

Plasma gun	SG-100 Plasma Gun (40kw Subsonic Mode)	
Powder feeder	127D Powder Feeder	
Anode part	145 forward injection	
Cathode part	129	
Gas injector	130 four holes	
	Ag layer	YBaCu–O layer
Plasma arc current (A)	600	900
Plasma arc voltage (V)	50	44
Arc gas: Ar (MPa)/ (standard $l\,min^{-1}$)	1.0/108.6	0.34/37.8
Arc gas: He (MPa)/ (standard $l\,min^{-1}$)	1.0/20.0	1.0/20.0
Carrier gas: Ar (MPa)/ (standard $l\,min^{-1}$)	0.41/7.5	0.34/5.6
Powder feed rate ($g\,min^{-1}$)	12	7.2
Scanning speed ($mm\,s^{-1}$)	100	100
Stand-off distance (mm)	100	100

TABLE II Layer arrangement of specimens

Layer	Material	Numbers of sub-layers	
		Specimen S-3	Specimen S-4
1	Ag	3	3
2	YBaCu–O	3	3
3	Ag	2	2
4	YBaCu–O	3	3
5	Ag	3	0

TABLE III Notations of specimens subjected to various heat treatments

Heat-treatment	Specimen S-3	Specimen S-4
As-sprayed	S-3-3	S-4-3
Ar pre-treatment	S-3-4	S-4-4
O_2 annealing	S-3-2	S-4-2
Ar pre-treatment + O_2 annealing	S-3-1	S-4-1

The densities of sprayed foils were measured by Archmedes' method in water using specimen S-3-3.

Specimen flexibility was evaluated by repeatedly bending the sprayed composite foil on to the surface of glass cylinders with various diameters, and then observing the foil surface using specimen S-3-3.

X-ray diffraction (XRD) examinations were carried out on the Y–Ba–Cu–O surfaces of specimens S-4 using a Philips X-ray generator model 1830.

The YBaCu–O surfaces of specimens S-4 and the silver surface of specimen S-3 were observed by scanning electron microscopy and local compositions were measured by Auger elemental spectroscopy (AES) using a PHI 660 scanning Auger microprobe.

Cross-sections of specimens S-4 were observed by optical and scanning electron microscopy. Local compositions were measured by energy despersive spectroscopy (EDS).

The superconductivity of specimens S-4 was determined magnetically using Quantum Design DC SQUID magnetometer. Specimens were cooled to 10 K at zero field and then heated under a constant applied magnetic field of 10 Oe.

3. Results

The thicknesses of sprayed foils measured using a micrometer were in the range 120–160 μm. The actual thicknesses measured from micrographs of cross-sections were in the range 100–120 μm.

Densities measured by Archmedes' method were around $7.5\,g\,cm^{-3}$, which corresponds to a porosity rate of around 15%.

The flexibility of sprayed foil is shown in Fig. 2. The functionally graded composite foil of silver and Y–Ba–Cu–O can be repeatedly bent on to a surface of a glass cylinder of 30 mm diameter. After 30 bending cycles, no cracking was found on the foil surface at × 10 magnification.

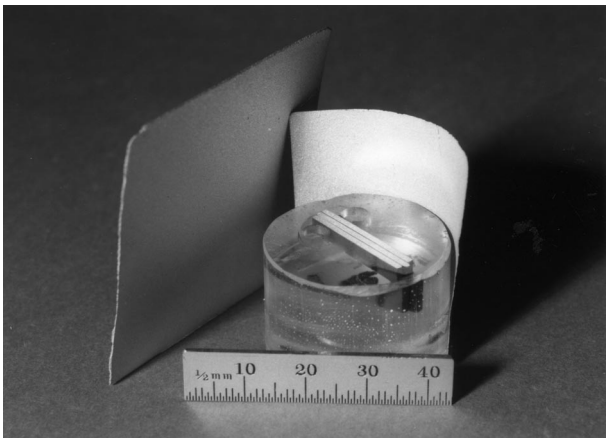

Figure 2 Functionally graded composite foils with a certain flexibility.

XRD patterns from specimens subjected to various heat treatments are shown in Fig. 3. The XRD pattern of Metco SC23 powder is also presented. The as-sprayed coating of Y–Ba–Cu–O does not contain Y123 phase (Fig. 3b), which was present in the Metco SC23 powder (Fig. 3a). The Y123 phase could not be recovered by argon pre-treatment. Major phases in the argon pretreated specimens are Y_2BaCuO_5 (Y211), $BaCuO_2$ (011), and minor amounts of oxides of copper (Fig. 3c). After oxygen annealing at 920 °C, the superconductor phase forms, but appears oxygen-deficient (i.e. the orthorhombic splitting of the characteristic peak at $2\theta = 32.5°–32.8°$ is not apparent, Fig. 3d). Specimens subjected to argon pre-treatment plus oxygen annealing show an improved orthorhombic splitting of the characteristic peak (Fig. 3e).

Figs 4–7 show the Y–Ba–Cu–O layer surfaces of the as-sprayed specimen and specimens subjected to various heat treatments (S-4). Fig. 8 shows the silver layer surface of the specimen with argon pre-treatment and oxygen annealing (S-3).

Complete melting of the as-sprayed layer with shrinkage micro-cracks are produced (Fig. 4). AES shows that the surface composition is yttrium, barium, copper and oxygen without silver. Enrichment of barium on the surface is observed, and the colour of surface is black.

Fig. 5 shows that during argon pre-treatment processing, silver in the underlayer is melted and penetrates through micro-cracks up to the YBaCu–O surface where it solidifies as small balls. AES detects small quantities of yttrium, barium and copper in silver balls. The background has the composition of yttrium, barium and copper with lower oxygen content compared with that on the surface of as-sprayed specimens. The morphology of the background surface shows little difference from that of the as-sprayed specimen, except that the colour of the surface changes from black to pink and the density of micro-cracks increases.

Fig. 6 shows the YBaCu–O surface of a specimen annealed in oxygen. The colour of the specimen is black. A large number of prism-like grains are produced during oxygen annealing. Many cavities can be observed between grains. The density of micro-cracks is lower than that in argon pre-treated specimens. AES shows that the surface has the composition of yttrium, barium, copper and oxygen without silver. The oxygen content is much higher than that in the specimen pre-treated in argon.

The colour of specimens pre-treated in argon plus annealed in oxygen changes from pink to black (Fig. 7). A large number of platelet-like grains and many rod-like grains are produced during the oxygen annealing after argon pre-treatment. The grain sizes are much larger than those in specimens only annealed in oxygen without argon pre-treatment (cf. Figs 6 and 7). AES shows that the platelet-like grains are composed of yttrium, barium, copper and oxygen while the rod-like grains have more yttrium. The oxygen content is much higher than that in the specimens only pre-treated in argon. Most small silver balls aggregate to larger particles and spread on the surface of the Y–Ba–Cu–O layer. EDS detects yttrium and less copper and barium in the silver particles.

Large areas of micro-cracks present in argon pre-treated specimens disappear, and much fewer new cracks occur. Fig. 8 shows the silver surface of the specimen argon pre-treated and oxygen annealed. The silver maintains a metal phase with a smooth surface without cracks.

Fig. 9 shows the cross-section of an as-sprayed specimen. Consistent with the surface observations, the sprayed splats are completely melted. Y–Ba–Cu–O layers are continuous and uniform. The porosity is low. The high porosity rate (15%) calculated from the measured density of the sprayed foil may be caused by the errors in measurement of the area ratio of silver to YBaCu–O.

Fig. 10 shows the cross-section of specimen pre-treated in argon. Silver is melted and penetrates into the Y–Ba–Cu–O layer. Two types of silver are observed: bounding one side of the micro-crack in the Y–Ba–Cu–O layer (Fig. 10b), and as small balls on the surface (Fig. 10a) which is consistent with surface observation. EDS shows small quantities of yttrium and less barium and copper in the silver phase. Numerous micro-cracks appear in cross-section.

Fig. 11 shows the cross-section of a specimen annealed in oxygen. In the Y–Ba–Cu–O layer, a high density of pores is formed during the annealing process. No trace of silver is detected by EDS in Y–Ba–Cu–O layer. This is consistent with the surface observations and indicates that silver does not melt nor penetrate into the Y–Ba–Cu–O layer during oxygen annealing even though the annealing temperature (920 °C) is 70 °C higher than that of argon pre-treatment (850 °C).

Fig. 12 shows the cross-section of specimen pre-treated in argon plus annealed in oxygen. Silver, which penetrates into the Y–Ba–Cu–O layer during argon pre-treatment, aggregates in larger particles and fills the cavities. Most micro-cracks formed in the Y–Ba–Cu–O layer of the argon pre-treated specimen disappeared, leaving some irregular-shaped cavities.

The d.c. magnetization curves of the as-sprayed specimen (S-4-3) and specimens subjected to argon

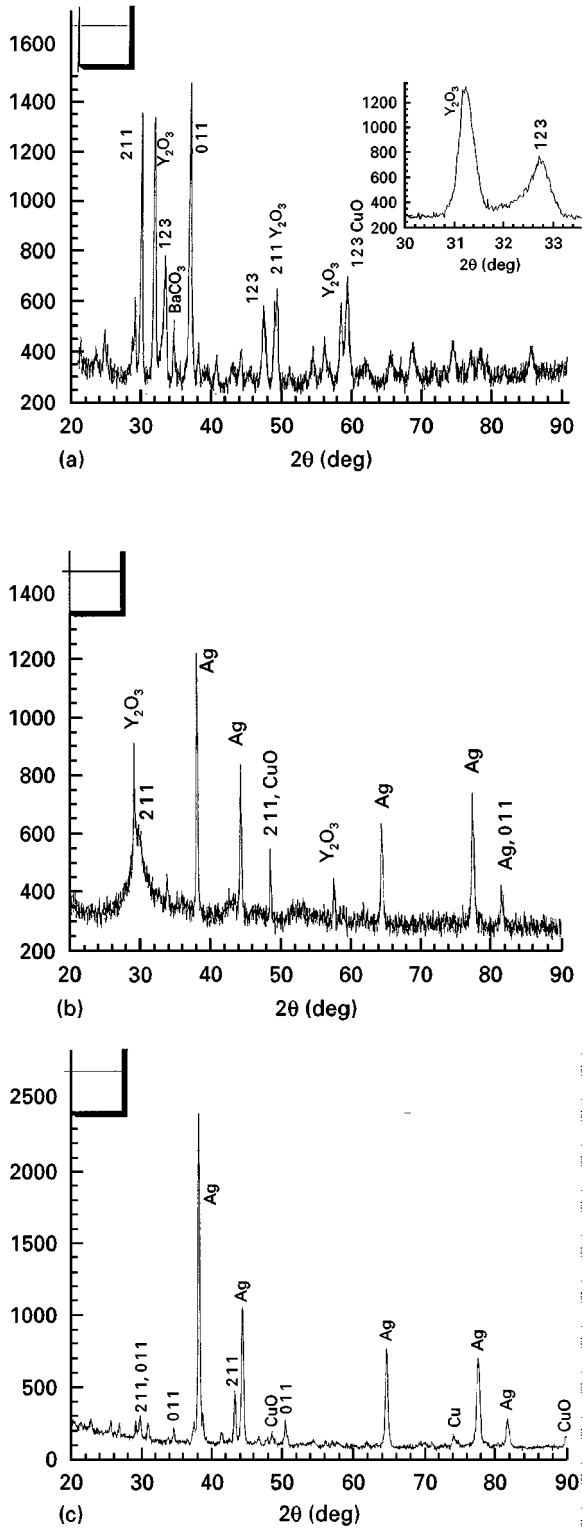

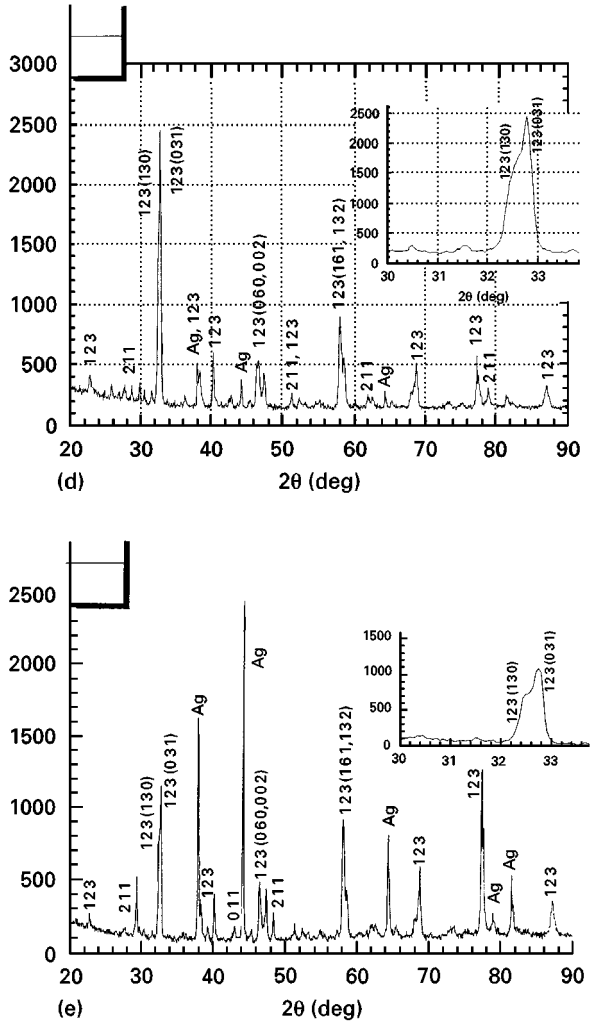

Figure 3 X-ray diffraction diagrams of (a) Metco SC23 $YBa_2Cu_{4.5}O_{7-\delta}$ powder, (b) S-4-3 as-sprayed, (c) S-4-4 argon pre-treated, (d) S-4-2 oxygen annealed, (e) S-4-1 argon pre-treated plus oxygen annealed specimens.

pre-treatment (S-4-4), oxygen annealing (S-4-2), and argon pre-treatment plus oxygen annealing (S-4-1) are shown in Fig. 13.

The as-sprayed specimen (S-4-3) and the specimen pre-treated in argon (S-4-4) are not superconducting. The specimen annealed in oxygen shows an onset of superconductivity at 89 K. The specimen pre-treated in argon plus annealed in oxygen shows an onset of superconductivity at 92 K. The wide transition widths of d.c. magnetization indicate small weak-linked grains.

4. Discussion

4.1. Recovery of superconductivity in sprayed foil

Fig. 3a shows the $YBa_2Cu_3O_{7-\delta}$ phase is present in SC23 spraying powder, but the unsplit peak at $2\theta = 32.5^\circ$ ((0 1 3) and (1 1 0)) is evidence of the non-superconducting tetragonal phase.

Fig. 3b shows that, in the XRD of as-sprayed specimens, none of the characteristic lines of $YBa_2Cu_3O_{7-\delta}$ appear, and this is confirmed by the SQUID results. The fact that as-sprayed coatings of the Y–Ba–Cu–O system are not superconducting is expected [10–15], and is caused by the rapid solidification of sprayed molten droplets which results in the formation of metastable phases [16].

Fig. 3c shows that, in specimens pre-treated in argon, the superconducting phase $YBa_2Cu_3O_{7-\delta}$ does not form. The surface and cross-section observations show that silver is melted and penetrates into the Y–Ba–Cu–O layer, yet the latter retains the original pattern, which means that no solid sintering reaction occurs during argon pre-treatment. The transformation which possibly occurs during argon pre-treatment is

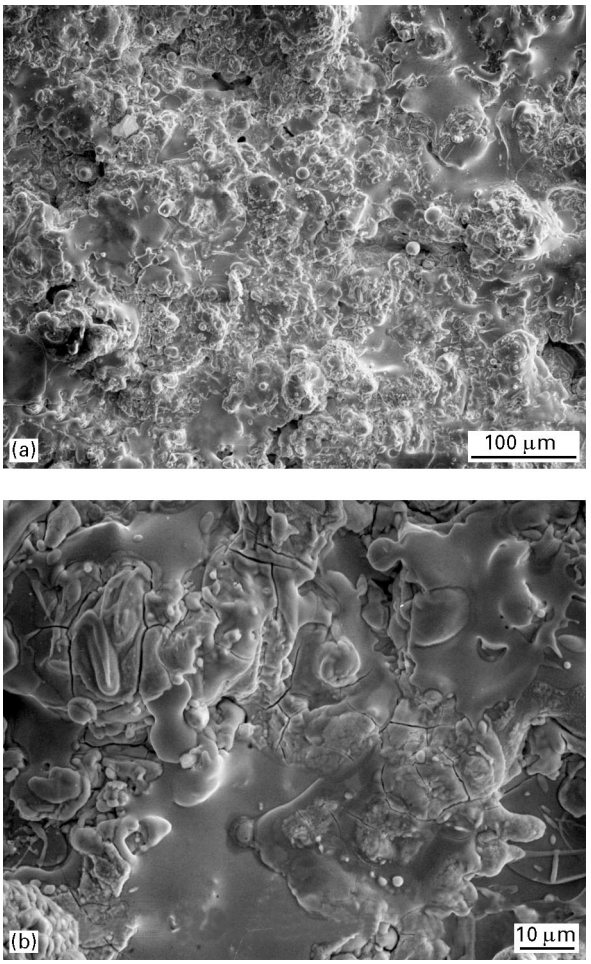

Figure 4 (a, b) YBaCu–O layer surface of an as-sprayed specimen.

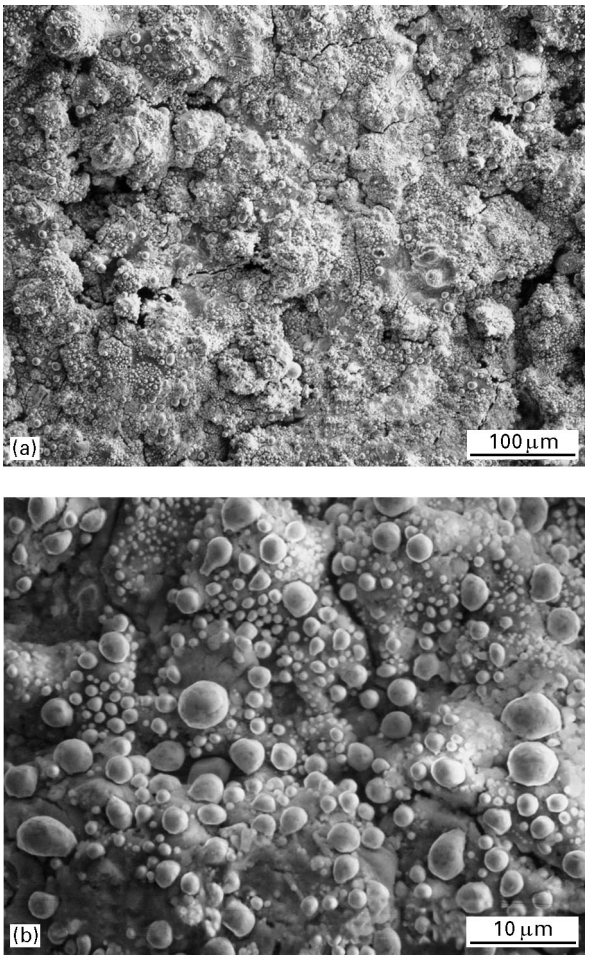

Figure 5 (a, b) YBaCu–O layer surface of a specimen pre-treated in argon.

that highly oxidized compounds like Y_2O_3 and CuO_2 and metastable phases transform to stable Y_2BaCuO_5 (2 1 1), $BaCuO_2$ (0 1 1), and reduced oxides of copper (CuO, Cu_2O) in an extremely low oxygen pressure atmosphere. The phases rich in copper and barium cause the pink colour of the specimen surface.

Fig. 3d shows that, in specimens annealed in oxygen, the superconductor phase $YBa_2Cu_3O_{7-\delta}$ forms, but the orthorhombic splitting at $2\theta = 32.5^\circ$ and 32.8° is not apparent. The SQUID results indicate a superconductivity onset at 89 K and a wide d.c. magnetization transition temperature range. The surface and cross-section observations show that the surface, although black in colour, is no longer smooth, but consists of a great number of small prism-like grains of Y123, 2–3 μm on edge, with a high porosity between the grains (Figs 6 and 11). There is no trace of residual liquid. Based on these facts, the prism-like grains are identified as $YBa_2Cu_3O_{7-\delta}$ superconductor phase and the most possible transformations are the solid sintering reactions between Y_2BaCuO_3, $BaCuO_2$, Y_2O_3, CuO and O_2 to form $YBa_2Cu_3O_{7-\delta}$ during annealing at 920 °C and then enrichment of oxygen by holding at 450 °C in flowing oxygen. The wide d.c. magnetization transition temperature range is caused by the fine grain sizes and low volume fraction of superconducting phase in the specimens which include silver layers and retained 2 1 1 and 0 1 1 phases.

For specimens pre-treated in argon and then annealed in oxygen, the following phenomena can be observed. The surface colour changes from pink to black. The relatively smooth surface of the YBaCu–O layer transforms to that which consists of a great number of small platelet-like grains ($2\,\mu m \times 6\,\mu m \times 10\,\mu m$) and rod-like grains ($2\,\mu m \times 2\,\mu m \times 10\,\mu m$) (Fig. 7). The grain sizes are much larger than that in specimens only annealed in oxygen (Fig. 6). The AES data show that the oxygen content is much higher than that in specimens only pre-treated with argon. XRD shows the presence of $YBa_2Cu_3O_{7-\delta}$ and more apparent orthorhombic splitting at $2\theta = 32.5$ and 32.8 °C (Fig. 3e). The magnetization measurements show a higher onset temperature for superconductivity (92 °C) and a slightly sharper initial transition (Fig. 13). The small silver balls on the surface and silver strips filling in the cracks in the Y–Ba–Cu–O layers which formed during argon pre-treatment aggregate into larger particles, filling in cavities or spreading on the surface (Figs 7a and 12).

Based on these observations, the platelet-like grains in the normal specimen S-4-1 are identified as $YBa_2Cu_3O_{7-\delta}$ phase and those in the rod-like grains as Y_2BaCuO_5. The transformations which form $YBa_2Cu_3O_{7-\delta}$ are verified to be liquid-phase sintering reactions [18], which increase the $YBa_2Cu_3O_{7-\delta}$ grain sizes. The transient liquid also plays a role in reducing microcracks which appear to be less numerous

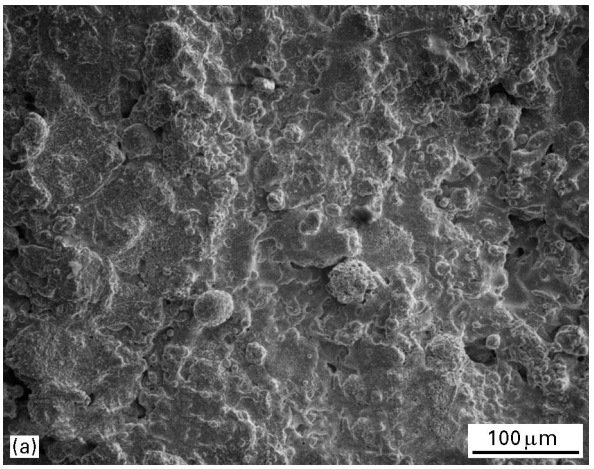

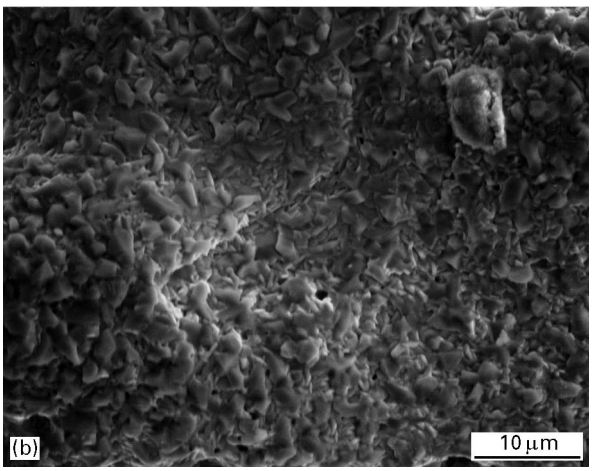

Figure 6 (a, b) YBaCu–O layer surface of a specimen annealed in oxygen.

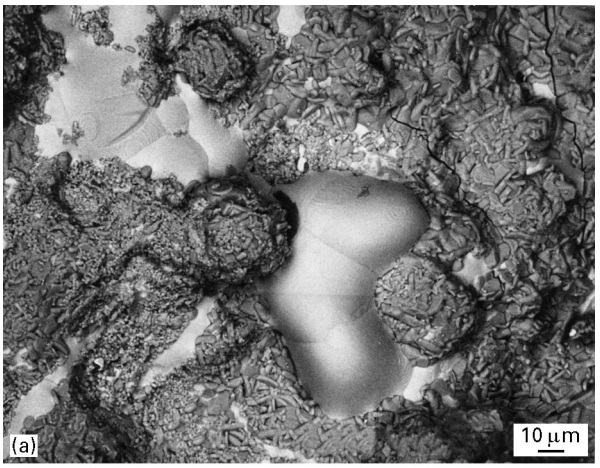

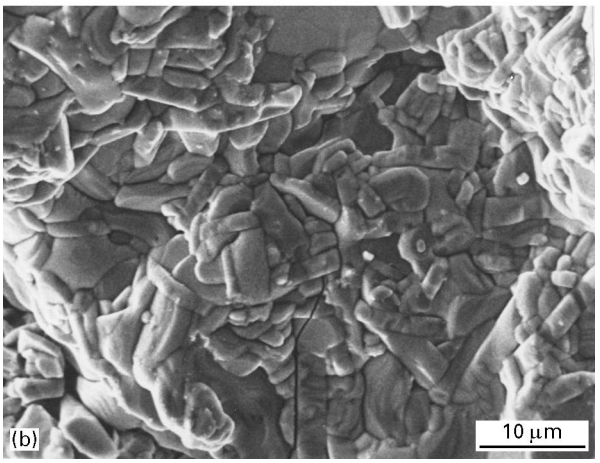

Figure 7 (a, b) YBaCu–O layer surface of a specimen pre-treated in argon plus annealed in oxygen.

after oxygen annealing than just after argon pre-treatment. The liquid is produced by the following reactions in the silver-doped Y–Ba–Cu–O system [2]

$$YBa_2Cu_3O_{7-\delta} + CuO = Y_2BaCuO_5 + L \quad (1)$$

$$BaCuO_2 + CuO = L \quad (2)$$

$$YBa_2Cu_3O_{7-\delta} + CuO + BaCuO_2 = L \quad (3)$$

The improvement of the orthorhombic splitting and superconducting transition are considered to be the results of the increase in size of platelet-like $YBa_2Cu_3O_{7-\delta}$ grains.

4.2. Behaviour and functions of silver

4.2.1. Melting and penetration into YBaCu–O layers

Part of the silver, close to the boundaries between silver and Y–Ba–Cu–O layers, melts at 850 °C during argon pretreatment but does not melt at 920 °C during oxygen annealing. Because EDS detects yttrium and less copper and barium in the silver balls on the surface of the argon pretreated specimen, and the silver particles spreading on the surface of the argon pretreated plus oxygen annealed specimen, the decrease in the melting temperature of part of the silver from 960 °C to less than 850 °C is apparently caused by dissolution of yttrium, copper and barium into the contacting layer of silver during argon pre-treatment.

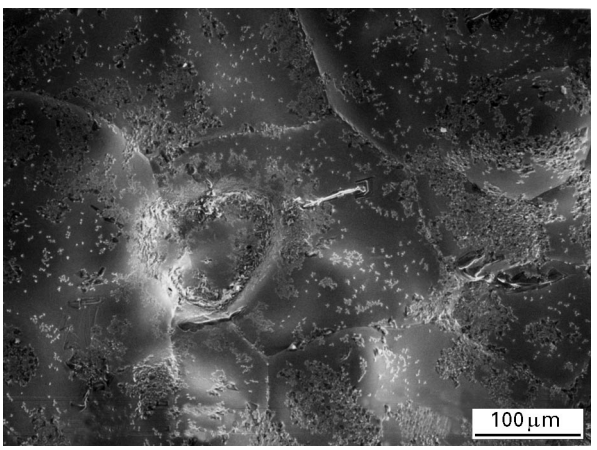

Figure 8 Silver layer surface of a specimen pre-treated in argon plus annealed in oxygen.

This process only occurs in an extremely low oxygen atmosphere. In the case of annealing in flowing oxygen, because any of the elements yttrium, barium and copper dissolved in silver will be oxidized by oxygen, only pure silver exists as solid phase.

At high temperature, silver wets the Y–Ba–Cu–O phase and penetrates into it through cavities and micro-cracks. In an argon atmosphere, at a temperature close to the melting point, the surface tension between silver and Y–Ba–Cu–O increases, and silver aggregates into small balls (Figs 5 and 10). In an

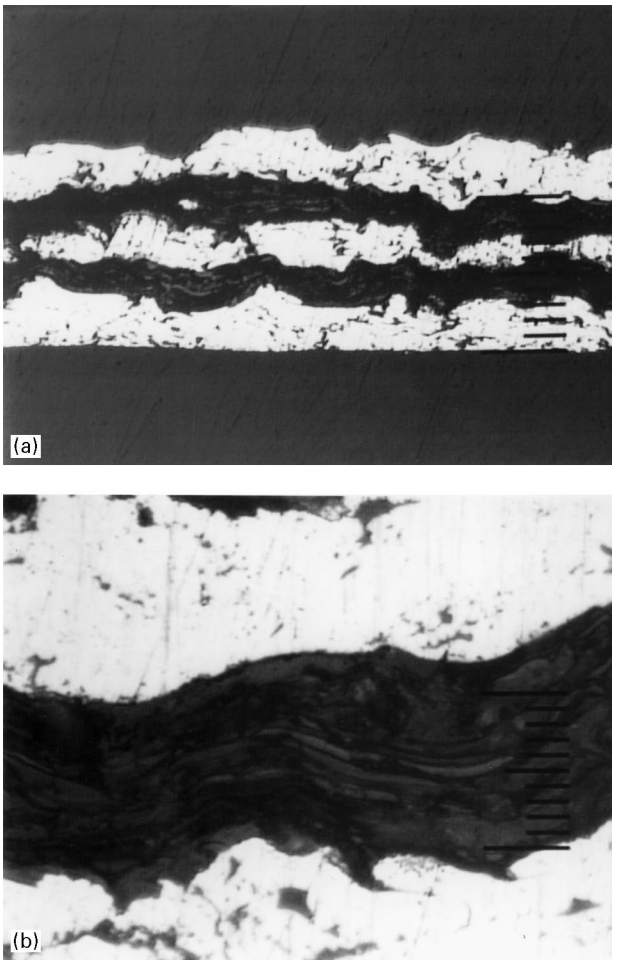

Figure 9 Cross-section of an as-sprayed specimen. (a) × 400, (b) × 2000.

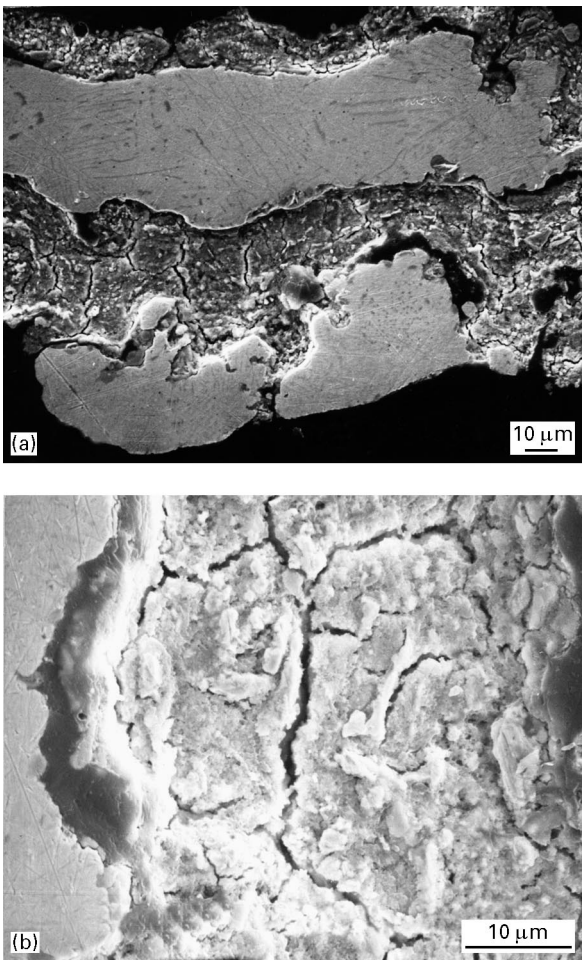

Figure 10 (a, b) Cross-section of a specimen pre-treated in argon.

oxygen atmosphere, the surface tension between silver and Y–Ba–Cu–O is still low, and silver aggregates into larger particles spreading on the surface (Figs 7 and 12).

4.2.2. Ductility enhancement

The functionally graded silver layers remarkably increase the ductility of the sprayed composite foils. Foils with a thickness of about 100 μm can be repeatedly (30 times) bent over a cylinder of 30 mm diameter (strain $\simeq 0.33\%$) without forming surface cracks.

Fig. 12 shows that silver fills the cavities formed in the YBaCu–O layer and makes it integrated. A more important effect of silver on the ductility is that it decreases the liquidation temperature. Therefore, partial liquidation occurs at the oxygen annealing temperature and heals most of the micro-cracks occurring in the argon pre-treated specimen (cf. Figs 10 and 12).

4.2.3. Improvement of superconductivity

Based on the above observations, it is thought that the beneficial effects of silver on the superconductivity are manifested through decreasing the liquidation temperature. The $YBa_2Cu_3O_{7-\delta}$ grain sizes in specimens argon pre-treated plus oxygen annealed are much larger than those of specimens only oxygen annealed. In the former, the silver melted and penetrated into the YBaCu–O layer during argon pre-treatment and $YBa_2Cu_3O_{7-\delta}$ superconductor phase forms in a partial liquidation condition during oxygen annealing. The larger grain sizes and the more apparent orthorhombic splitting result in a higher onset temperature of superconductivity. In the specimens which were only oxygen annealed, the silver remains in the solid phase and no molten phenomenon can be observed; $YBa_2Cu_3O_{7-\delta}$ superconductor phase is formed by a solid sintering process. The formed $YBa_2Cu_3O_{7-\delta}$ superconductor grains are smaller, the orthorhombic splitting is less apparent, and the superconductivity onset temperature is lower. Using results reported elsewhere [2] (Fig. 14), the effects of silver can be analysed. In the $YBa_2Cu_3O_{7-\delta}$–$BaCuO_{2+y}$–CuO system, Reactions 1, 2, and 3 can only be conducted at a temperature higher than 920 °C under 1 atm oxygen (Fig. 14a). In the $YBa_2Cu_3O_{7-\delta}$–$BaCuO_{2+y}$–CuO–Ag system, these reactions can be conducted at a temperature lower than 920 °C (Fig. 14b). The similar grain sizes obtained in this work (920 °C) and elsewhere [16] (950 °C) indicate that the doping of silver lowers the temperatures for the appearance of liquids by 30 K.

4.3. Further work on melt-texture treatment

The randomly oriented grains shown in Fig. 7 and the weak links between grain boundaries with micro-

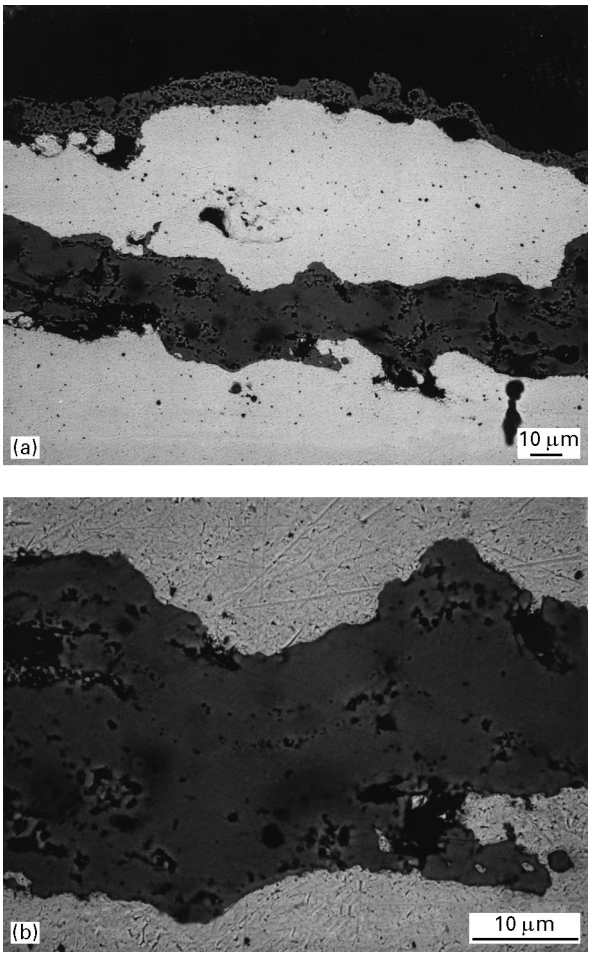

Figure 11 (a, b) Cross-sections of specimens annealed in oxygen.

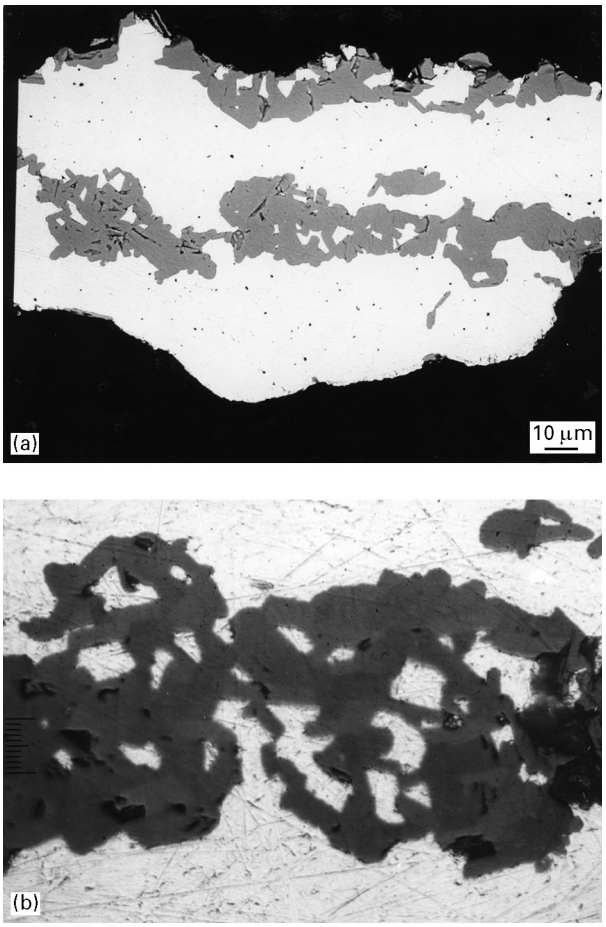

Figure 12 (a, b) Cross-sections of specimens pre-treated in argon plus annealed in oxygen.

cracks must result in a low critical transport current, which is estimated, by d.c. magnetization, to be as low as several hundreds of amperes per square centimetre or less. For improving the critical current and healing the micro-cracks, a partial melt-texture process should be conducted at a temperature higher than that of the peritectic reaction

$$YBa_2Cu_3O_{7-x} = Y_2BaCuO_5 + L \qquad (4)$$

For the functionally graded foil of $YBa_2Cu_3O_{7-\delta}$ and silver the partial melt-texture temperature must be lower than the melting point of silver (960 °C). According to Fig. 14b, for the $YBa_2Cu_3O_{7-\delta}$–$BaCuO_{2+y}$–CuO–Ag system this can be realized at a partial oxygen pressure of 10^{-2} atm.

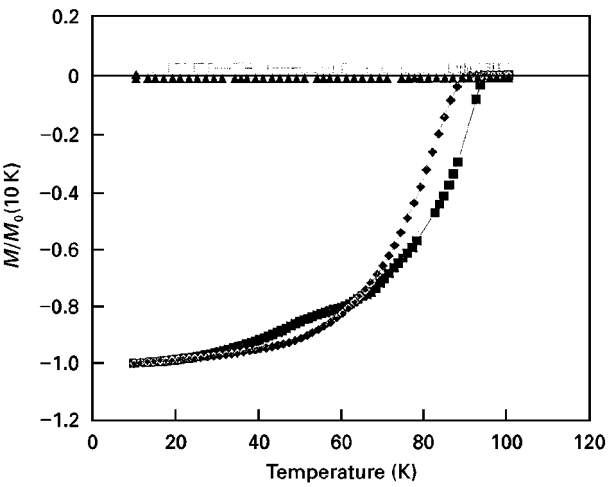

Figure 13 D.c. magnetization transition curves measured by a d.c. SQUID magnetometer, of specimens (▲) S-4-3 as-sprayed (□) S-4-4 argon pre-treated, (◆) S-4-2 oxygen annealed (■) S-4-1 argon pre-treated plus oxygen annealed. M is the magnetization measured at T and M_0 is the magnetization measured at 10 K.

5. Conclusions

1. Functionally graded composite foils of YBaCu–O and silver with certain flexibility can be produced by air plasma spraying.

2. Superconductivity with an onset temperature of 89–92 K is present in specimens after annealing in flowing oxygen and is improved by pre-treatment in argon. Argon pre-treatment results in a partial liquidation during the subsequent oxygen annealing, which increases the grain sizes of $YBa_2Cu_3O_{7-\delta}$ superconductor phase and its orthorhombic splitting.

3. Graded silver layers effectively increase the ductility of sprayed YBaCu–O foil and fill cavities in the YBaCu–O layer after melting during the processes of argon pre-treatment and oxygen annealing. Silver improves the superconductivity by decreasing the partial liquidation temperature which increases the grain sizes of the $YBa_2Cu_3O_{7-\delta}$ superconductive phase and its orthorhombic splitting.

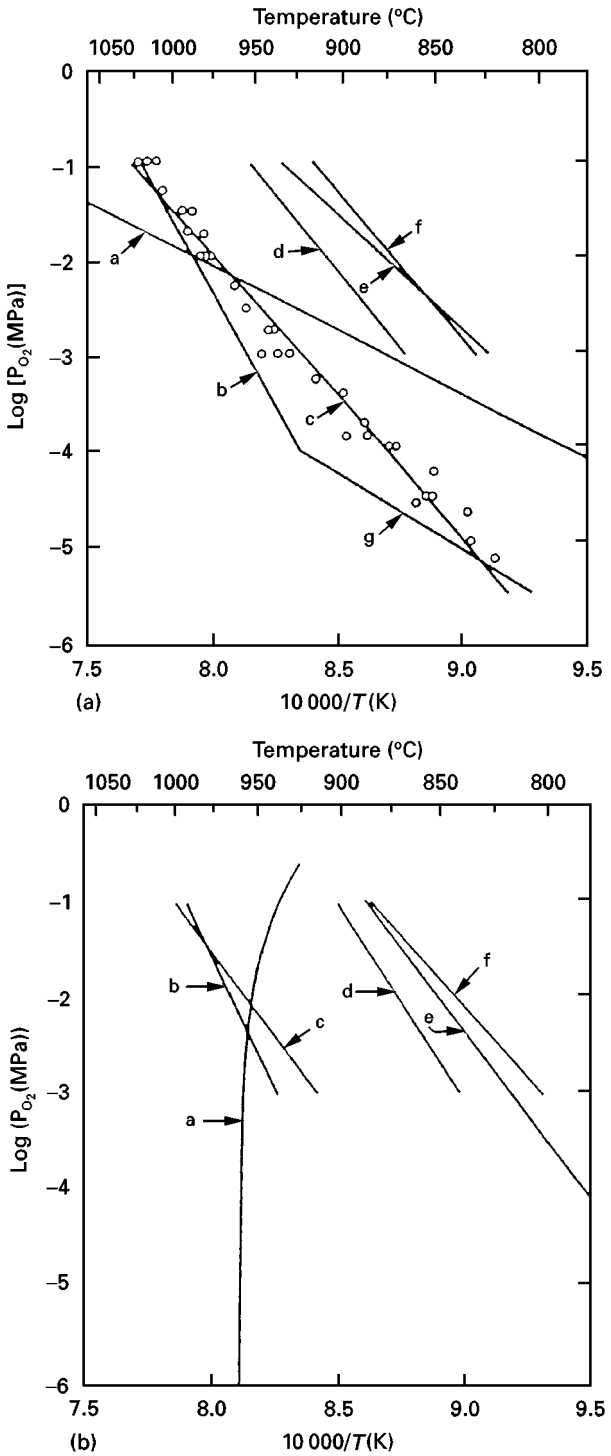

Figure 14 Calculated T–pO_2 characteristics for several equilibria in the (a) $YBa_2Cu_3O_{7-x}$–$BaCuO_{2+y}$–CuO and (b) $YBa_2Cu_3O_{7-\delta}$–$BaCuO_{2+y}$–CuO–Ag systems [2]. (a) 1, $CuO \rightleftharpoons Cu_2O + O_2$; 2, $123 \rightleftharpoons 211 + L$; 3, $011 \rightleftharpoons L$; 4, $123 + CuO \rightleftharpoons 211 + L$; 5, $011 + CuO \rightleftharpoons L$; 6, $123 + CuO + 011 \rightleftharpoons L$; 7, $123 \rightleftharpoons 211 + 012 + 132$. (b) 1, Ag–O eutectic; 2, $123 \rightleftharpoons 211 + L$; 3, $011 \rightleftharpoons L$; 4, $123 + CuO \rightleftharpoons 211 + L$; 5, $011 + CuO \rightleftharpoons L$; 6, $123 + CuO + 011 \rightleftharpoons L$.

4. Further work on the partial melt-texture treatment is necessary to improve the critical transport current of $YBa_2Cu_3O_{7-\delta}$ superconductor phase in functionally sprayed composite foils with silver graded layers.

Acknowledgements

The authors thank R. W. McCallum, S. Chumbley, K. W. Dennis, F. Labbs, T. E. Bloomer, H. E. Sailsbury, C. Schwichtenberg and J. Williams, Ames Laboratory, for their help and advice on experiments. The authors also thank R. A. Sampath and R. A. Neiser Jr, SUNY at Stony Brook, offering the SC23 powder. This work was supported by the US Department of Energy under contract W-7405-ENG-82.

References

1. M. KOIZUMI, in "Proceedings of the 2nd International Symposium on Functionally Gradient Materials" (The American Ceramic Society, 1992) p. 1.
2. T. B. LINDEMER, F. A. WASHBURN and C. S. MACDOUGALL, *Physica C* **196** (1992) 390.
3. M. J. DAY, S. D. SUTTON, F. WELLHOFER and J. S. ABELL, *Supercond. Sci. Technol.* **6** (1993) 96.
4. E. YANMAZ, I. H. MUTLU, T. KUCUKOMEROGLU and M. ALTUNBAS, *ibid.* **7** (1994) 903.
5. J. C. BOWKER and I. I. WHITLOW, *ibid.* **6** (1993) 106.
6. C. C. TSUEI, C. C. CHI, T. FREY, D. B. MITZI, T. KAZYAKA, T. HAUGAN, J. YE, S. PATEL, T. SHAW and M. K. WU, *Mater. Chem. Phys.* **32** (1992) 95.
7. J. P. TRAVERSE, P. ROUX, J. C. BRESSOLLES, E. SNOECK and C. ROUCAU, *Supercond. Sci. Technol.* **6** (1993) 573.
8. J. P. TRAVERSE, C. RUAU, P. ROUX, J. C. BRESSOLLES, E. SNOECK and C. ROUCAU, *ibid.* **7** (1994) 353.
9. G. E. JANG and K. MUKHERJEE, *ibid.* **7** (1994) 344.
10. Y. ARATA, A. OHMORI and S. SANO, in "Proceedings of the National Thermal Spray Conference-87" (ASM International, 1987) p. 183.
11. R. A. NEISER, J. P. KIRKLAND, W. T. ELAM, E. F. SKELTON, H. HERMAN, G. A. BANCKE, S. SAMPATH, D. GANSERT and H. G. WANG, *ibid.*, p. 195.
12. W. D. WILBER and J. D. REARDON, in "Proceedings of the National Thermal Spray Conference-88" (ASM International, 1988) p. 227.
13. D. J. VARACALLE Jr, K. L. TELSCHOW, R. N. WRIGHT and J. C. DEBSIKDAR, *ibid.*, p. 211.
14. K. KUMAR and A. PETROVICH, *ibid.*, p. 219.
15. J. KARTHIKEYAN, R. RATNARAJ, A. J. HILL, Y. C. FAYMAN and C. C. BERNDT, in "Proceedings of the National Thermal Spray Conference-91" (ASM International, 1991) p. 497.
16. R. A. NEISER, PhD Thesis, State University of New York at Stony Brook (1989).
17. H. WANG, H. HERMAN, H. J. WIESMANN, Y. ZHU, Y. W. XU, R. L. SABATINI and M. SUENAGA, *Appl. Phys. Lett.* **57** (1990) 2495.
18. J. H. CHEN, M. F. BESSER, R. K. TRIVEDI, M. J. KRAMER and D. J. SORDELET, *J. Mater. Sci. Lett.* **16** (1997) 988.

Received 27 January 1997
and accepted 18 March 1998